**Rare Metal Materials and Engineering**
Volume 51, Issue 8, August 2022
Available online at www.rmme.ac.cn

Science Press

**Cite this article as**: Jia Yuzhen, Hou Yaqing, Wang Pengfei, et al. Effect of Al on Microstructure and Corrosion Behavior of Low Neutron Absorption Cross-Section Ti-Zr-Nb High Entropy Alloys[J]. Rare Metal Materials and Engineering, 2022, 51(08): 2822-2829.

ARTICLE

# Effect of Al on Microstructure and Corrosion Behavior of Low Neutron Absorption Cross-Section Ti-Zr-Nb High Entropy Alloys

**Jia Yuzhen[1], Hou Yaqing[2], Wang Pengfei[1], Zhang Wei[1], Dai Xun[1]**

*[1] Science and Technology on Reactor Fuel and Materials Laboratory, Nuclear Power Institute of China, Chengdu 610213, China; [2] Material Digital R&D Center, China Iron & Steel Research Institute Group, Beijing 100081, China*

**Abstract:** The effect of Al on the microstructure and corrosion behavior of low neutron absorption cross-section Ti-Zr-Nb high entropy alloys was investigated. The phase diagram, microstructure, oxidation behavior and corrosion behavior of Ti-Zr-Nb alloys without Al addition and with ~15at% Al were compared. The phase diagram shows that below the melting temperature, Ti-Zr-Nb ternary alloys are bcc phase, and Al is inclined to form intermetallics in Ti-Zr-Nb alloys, and thus reduces the single-phase bcc temperature region in phase diagram. XRD and TEM results show that as-cast Ti-Zr-Nb ternary alloys is simple bcc structure, and Al will transform the crystal structure to ordered B2 structure. The corrosion behavior of Ti-Zr-Nb alloys was studied by thermogravimetric analysis and autoclave exposure. Results show that corrosion oxide layer formed on TiZrNb ternary alloys tends to spall during corrosion process, while Al addition will increase the stability of oxide layer without changing the main type of oxide formed during corrosion process. Oxidation kinetics was evaluated by calculating reaction rate constants and activation energies, and it is found that the high temperature oxidation property of Ti-Zr-Nb alloys with Al addition is comparable to that of Zr alloys.

**Key words:** Ti-Zr-Nb alloy; aluminum; high entropy alloy; corrosion; oxidation

The concept of accident tolerant fuel (ATF) was proposed to achieve higher safety margins under accident scenarios[1]. During the last two decades, a new group of alloys, high-entropy alloys (HEAs), has attracted much attention due to their attractive properties[2]. Compared to conventional alloys, HEAs are designed with a completely new strategy, with three or more principal elements in equal or near-equal concentrations as alloying elements. HEAs have advantages in many fields, such as high strength[3], irradiation resistance[4], corrosion and oxidation resistance[5,6]. The combination of good corrosion resistance and excellent irradiation resistance makes HEAs potential candidates for ATF cladding materials.

Among HEAs, refractory high-entropy alloys (RHEAs) are one of the most latest developments in structural materials. These alloys have promising high-temperature mechanical properties and improved oxidation resistance compared to conventional refractory alloys[7]. It has been shown that more than half of published RHEAs contain equiatomic concentration of Nb, Ti and Zr[8]. RHEAs composed of Ti, Zr, Nb and other elements show excellent radiation and corrosion resistance, making it promising cladding materials in nuclear reactors[9,10]. In addition, the neutron absorption cross-sections ($S_a$) of Nb, Ti, Zr elements are acceptable when used as cladding materials, compared to some other refractory metal elements such as Hf, Ta, W. Therefore, Ti-Zr-Nb HEAs have the potential to be used as ATF material in future.

Addition of Al element may have a profound effect on the microstructure and properties of HEAs. First of all, Al may change the phase of HEAs, which may lead to great change of the properties[11,12]. Al addition also has a profound effect on the corrosion resistance of HEAs, which may be beneficial or detrimental[13-15]. However, the corrosion behavior and oxidation behavior of Ti-Zr-Nb alloys were rarely investigated in the past.

Received date: August 04, 2021
Foundation item: CNNC Science Fund for Talented Young Scholars (2018-05)
Corresponding author: Jia Yuzhen, Ph. D., Associate Researcher, Science and Technology on Reactor Fuel and Materials Laboratory, Nuclear Power Institute of China, Chengdu 610213, P. R. China, Tel: 0086-28-85903839, E-mail: jaja880816@aliyun.com

Copyright © 2022, Northwest Institute for Nonferrous Metal Research. Published by Science Press. All rights reserved.

In this study, Ti-Zr-Nb HEA alloys with different contents of Al were designed and prepared, and the microstructure, oxidation behavior and corrosion behavior were investigated. The effect of Al on the microstructure and corrosion behavior of Ti-Zr-Nb HEAs was discussed. The results of present study will shed new light on the corrosion behavior of HEAs.

## 1 Calculation

### 1.1 Alloy search and prediction

The ability for elemental mixtures to form a single-phase solid solution was assessed by calculating the empirical parameters of HEAs formation. The empirical parameters include the entropy of mixing ($\Delta S_{mix}$), the enthalpy of mixing ($\Delta H_{mix}$), the atomic size difference ($\delta$), parameter $\Omega$, etc[16].

$$\delta = \sqrt{\sum_{i=1}^{n} c_i \left(1 - \frac{r_i}{\bar{r}}\right)^2} \quad (1)$$

$$\bar{r} = \sum_{i=1}^{n} c_i r_i \quad (2)$$

Parameter $\Omega$ can be defined:

$$\Omega = T_m \Delta S_{mix} / \Delta H_{mix} \quad (3)$$

$$T_m = \sum_{i=1}^{n} c_i (T_m)_i \quad (4)$$

In a multi-component HEA system, for the formation of single phase solution phase, it is indicated that $\delta \leqslant 6.6\%$ and $\Omega \geqslant 1.1$ are required to form a solid solution[16].

The composition of Ti-Zr-Nb HEAs studied in this research was designed and calculated, as shown in Table 1. Neutron absorption cross-section ($S_a$) is an important parameter for nuclear materials, such as cladding materials and grid spacers, in reactors. For those structure materials, the lower neutron absorption cross-section is necessary. Therefore, in this research, Ti-Zr-Nb HEAs with low neutron absorption cross-section were designed compared to traditional refractory HEAs. The neutron absorption cross-sections of the alloys investigated are all about $2\times10^{-24}$ cm$^2$. TiZrNb alloy (TZN1) has the highest $S_a$, about $2.36\times10^{-24}$ cm$^2$. $Ti_{0.75}ZrNbAl_{0.5}$ alloy (Al0.5-TZN2) has the lowest $S_a$, about $1.77\times10^{-24}$ cm$^2$. The entropy of alloys was calculated as well. All alloys can be classified as HEAs in a general sense. Most of the alloys have entropy around $1.0R$~$1.5R$ ($R$=8.314 J/(mol·K)), and the entropy of Al0.5V0.25-TZN2 is $1.51R$. For all alloys, parameter $\delta$ and $\Omega$ satisfied the HEA formation criterion ($\Omega \geqslant 1.1$ and $\delta \leqslant 6.6\%$).

### 1.2 Calculation of phase diagram

In order to investigate the phase and microstructure of HEAs, calculation of phase diagram (CALPHAD) method was performed in Thermocalc™ using the HEA database "TCHEA4"[17]. The equilibrium phases of HEAs were predicted from 200 °C to 2000 °C.

## 2 Experiment

### 2.1 Magnetic levitation melting

Alloys were prepared by weighing the pure elements according to their target stoichiometries to a total of ~1 kg. A mixture of pure metals (purity≥99.9wt% ) was melted and solidified in a magnetic levitation melting furnace at $10^{-3}$ Pa vacuum and Ar partial pressure of $10^{-1}$ Pa. Raw metals were completely melted at applied current of 300~450 A, and then cast in a mold with dimensions of $\Phi$60 mm×60 mm. The ingots were remelted for 3~5 times and flipped each time to homogenize its chemical composition.

### 2.2 Microstructure characterization

Samples for scanning electron microscope (SEM) observation were prepared by mechanical polishing, and slightly corroded for a few seconds with a diluted Kroll reagent. SEM analysis was conducted on NOVA NANO SEM 400 equipped with an energy dispersive X-ray spectroscopy (EDS) detector. Transmission electron microscopy (TEM) samples were prepared by ion thinning on Leica EM RES102, and analyzed on FEI Tecnai G2 F20. ARL EQUINOX 3000 X with Cu-Kα X-ray source was used to collect reflections on a rotating stage.

### 2.3 Property test

Indentation hardness was obtained on INNOVATEST FALCON 500 Vickers hardness tester using a diamond Vickers tip. All indents were made at 4.9 N for 15 s.

An autoclave test was performed in a static autoclave in pure water <45 μg/kg oxygen at 360 °C and a saturation pressure of 18.6 MPa. Mass gain measurements were used to assess the corrosion resistance.

In this work, high-temperature oxidation tests for HEAs were performed using a thermogravimetric analyzer (TGA, SETARAMSETSYS, France) in flowing steam environment at 600, 800, 1000 and 1200 °C for 7200 s to simulate the LOCA condition of nuclear reactor. The test coupon was mounted in Pt hanger inside the furnace and heated from ambient temperature to the setting temperature at a rate of 50 °C/min. Meanwhile, the 99.99% Ar gas was flowed into the chamber at the speed of 20 mL/min to prevent the initial oxidation during the temperature ramp. After the temperature reached to the setting temperature, the mixed gas of Ar and water vapor with the 90% humidity flowed concurrently into the chamber at the same rate of 20 mL/min. The specimen was isothermally oxidized in the steam environment at a setting temperature for 7200 s, and then was cooled to ambient temperature in Ar gas environment.

## 3 Results and Discussion

Predictions from CALPHAD are now presented and discussed. Fig.1 shows the predicted phases and their fractions under equilibrium conditions, at 200~2000 °C for TZN1, V0.25-TZN2, Al0.5-TZN1, Al0.5V0.25-TZN2 alloys. In agreement with the prediction of empirical parameters calculation, a single-phase bcc region is predicted below the melting temperature for the alloys, and the bcc phase is stable over the temperature range. For TZN1 and V0.25-TZN2, single-phase bcc regions are quite broad, and bcc structure can be stable at 700~1700 °C. Below 700 °C, TZN1 and V0.25-TZN2 alloys will be decomposed to two bcc phases with the same lattice structure and different composition due to

**Table 1 Chemical composition design and the empirical parameters of Ti-Zr-Nb alloys**

| Alloy | Content/at% | | | | | $S_a$/× $10^{-24}$ $cm^2$ | Entropy/$R$ | $\delta$/% | $\Omega$ |
|---|---|---|---|---|---|---|---|---|---|
| | Ti | Zr | Nb | Al | V | | | | |
| TiZrNb (TZN1) | 33.3 | 33.3 | 33.3 | 0 | 0 | 2.36 | 1.10 | 5.0 | 7.79 |
| Ti0.75ZrNb (TZN2) | 27.2 | 36.4 | 36.4 | 0 | 0 | 2.07 | 1.10 | 5.1 | 7.08 |
| TiZrNbAl0.5 (Al0.5-TZN1) | 28.6 | 28.6 | 28.6 | 14.3 | 0 | 2 | 1.35 | 4.9 | 1.80 |
| Ti0.75ZrNbAl0.5 (Al0.5-TZN2) | 23.1 | 30.8 | 30.8 | 15.4 | 0 | 1.77 | 1.35 | 5.0 | 1.70 |
| Ti0.75ZrNbV0.25 (V0.25-TZN2) | 25 | 33.3 | 33.3 | 0 | 8.3 | 2.32 | 1.29 | 6.0 | 13.97 |
| Ti0.75ZrNbV0.25 Al0.5 (Al0.5V0.25-TZN2) | 21.4 | 28.6 | 28.6 | 14.3 | 7.1 | 2.02 | 1.51 | 5.7 | 1.61 |

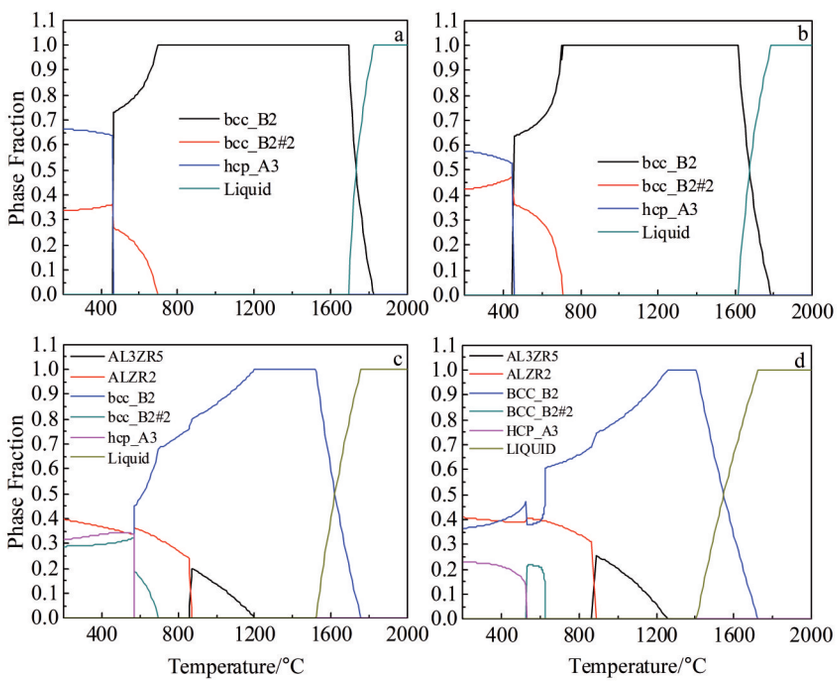


Fig.1 Predicted equilibrium phase diagrams of TZN1 (a), V0.25-TZN2 (b), Al0.5-TZN1 (c), and Al0.5V0.25-TZN2 (d) at 200~2000 °C

spinodal decomposition. The phase diagrams of TZN1 and V0.25-TZN2 alloys are quite similar, which indicates that a small addition of V will not significantly influence the phase composition and microstructure. Moreover, V addition will increase the entropy of HEAs, which may promote the properties of the alloys. For Al0.5-TZN1 and Al0.5V0.25-TZN2, Al is added in Ti-Zr-Nb HEAs. The phase diagrams show that Al and Zr are inclined to form intermetallics with different stoichiometries, which reduces the single-phase bcc temperature region. The boundary at which this single-phase is separated into a dual phase microstructure is predicted to occur at 1200 and 1250 °C for Al0.5-TZN1 and Al0.5V0.25-TZN2, respectively. At lower temperatures (<700 °C), for all alloys studied, $\alpha$ phase (hcp structure) is predicted, which is promoted by the allotropic transformations for Ti and Zr.

The SEM morphologies (Fig. 2) reveal a typical dendritic microstructure for the magnetic levitation melted as-cast samples of Ti-Zr-Nb alloys. The elemental distribution in the

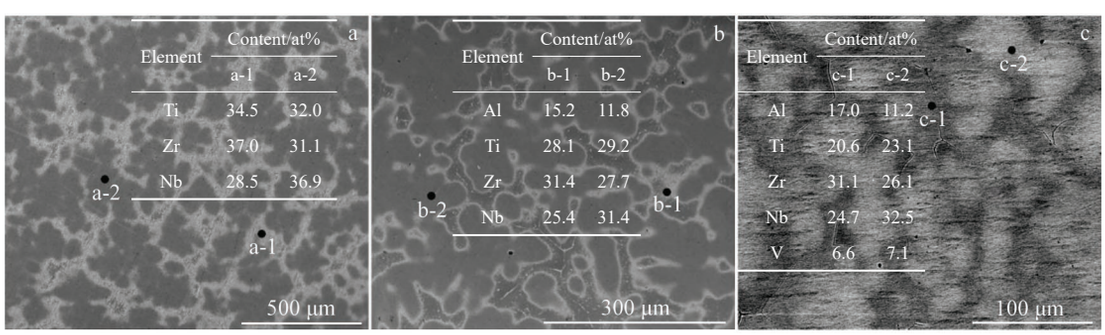


Fig.2 SEM morphologies and EDS results of the dendritic phase and inter-dendritic regions for different Ti-Zr-Nb alloys: (a) TZN1, (b) Al0.5-TZN1, and (c) Al0.5V0.25-TZN2

dendrite and inter-dendritic regions of Ti-Zr-Nb samples was characterized by EDS. The chemical compositions of the dendritic phase and inter-dendritic regions are close to the designed composition. From EDS analysis, it is clear that the dendritic phase and inter-dendritic regions are predominantly composed of (Nb, Ti) and (Zr, Al), respectively. This is mainly because the rate of atom diffusion cannot keep up with the crystallization process caused by the chemical segregation formed during solidification, with the predominant segregation of the refractory elements (mainly Nb) in the dendrites and the lower melting temperature elements (i.e. Al) in the inter-dendrites. In addition, Zr and Al tend to segregate simultaneously, which is mainly due to the low mixing enthalpy of these two elements (−44 kJ/mol)[18].

Fig.3 shows the XRD patterns of Ti-Zr-Nb alloy samples in the as-cast state. The XRD patterns show that all alloys possess a bcc structure, with a little difference in lattice parameter due to different compositions. As for TZN1 and TZN2 alloys, the Bragg diffraction peaks correspond to the bcc phase, with a strong {110} bcc diffraction peak and the lattice parameter around 0.34 nm. With addition of V, diffraction pattern of V0.25-TZN2 alloy is similar to that of TZN1 and TZN2 alloys, which indicates a bcc crystal structure. However, after Al addition, the diffraction patterns of Al0.5-TZN1, Al0.5-TZN2, Al0.5V0.25-TZN2 show the superlattice reflection peak of (001), (111) and (210) bcc located at about 27° , 47° and 62° (the diffraction peaks labeled in blue in Fig. 3), respectively, which indicates an ordered bcc (B2: TiAl type, space group Pm3m) phase. From the results shown above, it can be seen that the addition of Al in Ti-Zr-Nb alloys will change the crystal structure from simple bcc structure to ordered B2 structure. This may be because Al atoms are located in some certain lattice positions forming superlattice. This kind of ordering has been observed and researched in many kinds of HEAs, and it is believed that the ordering of the microstructure has a profound effect on the deformation mechanism and mechanical properties of HEAs [19].

The Al-induced ordering of the microstructure was also confirmed by TEM, as shown in Fig. 4. Fig. 4 shows bright-field TEM images and corresponding selected area electron diffraction (SAED) patterns of TZN1 alloy and Al0.5-TZN1 alloy samples. As seen in Fig. 4a, (001) diffraction spot does not appear in the SAED pattern along the [001] zone axis, which confirms the bcc structure of TZN1 alloy. On the contrary, SAED pattern shows the presence of (100) superlattice maxima which suggests the ordering of B2 phase. The TEM finding is consistent with the XRD data.

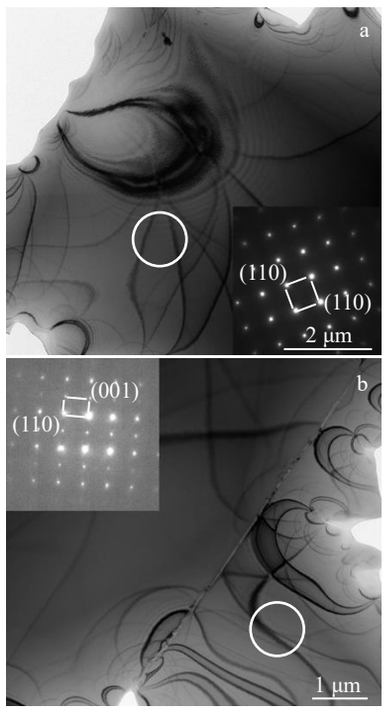


Fig.4 TEM bright field images and SAED pattern of TZN1 alloy (a) and Al0.5-TZN1 alloy (b)

The microhardness of as-cast samples of different Ti-Zr-Ni alloys was analyzed, as shown in Fig. 5. From the results, it can be seen that the hardness HV of TZN1 and TZN2 alloys is about 2450 MPa, which is lower than that of other alloys. For V0.25-TZN2 alloy, V addition cannot increase hardness of alloys a lot, and it is in agreement with the microstructure analysis, which implies that V cannot change the microstructure and hardness of Ti-Zr-Nb alloys. For Ti-Zr-Nb alloys

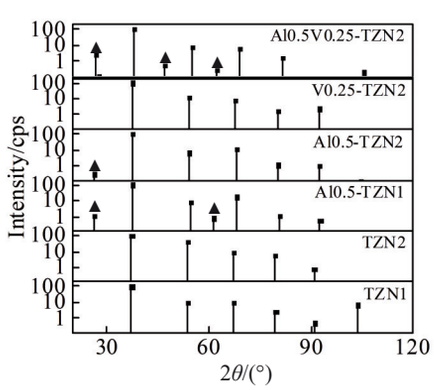


Fig.3 XRD patterns of different Ti-Zr-Nb alloys

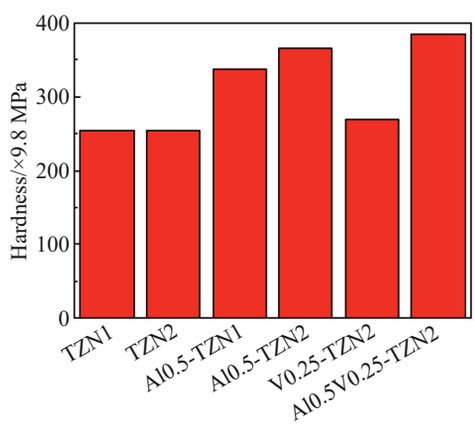


Fig.5 Microhardness of different Ti-Zr-Nb HEAs

with addition of Al element, microhardness can be increased by 32%~51%. Therefore, Al element is effective to increase the hardness of Ti-Zr-Nb alloys. This is mainly because Al changes the crystal structure of Ti-Zr-Nb alloys. Microstructure characterization results show the Al-induced ordering of the microstructure. In previous studies, the ordering will promote the mechanical properties of HEAs, and the chemical fluctuation will make the HEAs have high strength and ductility[20].

Mass gain measurements of the Ti-Zr-Nb alloys oxidized in steam are shown in Fig. 6, which shows the different growth rates at 600, 800, 1000 and 1200 °C. Fig. 6a shows the mass gain measurements of the TZN1 and TZN2 alloys at 800 °C. At the beginning of the oxidation process, the mass of the samples increases for a short time, and then the mass decreases continuously with the exposure time. It is the same for the oxidation behavior of the TZN1 and TZN2 alloys at 600 and 1000 °C in steam. The mass reduction during the oxidation process is mainly due to the spallation of the oxidation layer on sample surface, as can been seen from the surface morphology shown in Fig. 7. With the addition of Al, for Al0.5-TZN1 and Al0.5V0.25-TZN2 alloys, the oxidation behavior in steam is very similar, and the mass gain of the samples increases gradually during the oxidation process as shown in Fig. 6b. After oxidation test in steam at 600, 800, 1000 and 1200 °C for 2 h, the oxidized surface of Al0.5-TZN1 and Al0.5V0.25-TZN2 alloys keeps integrity, as shown in Fig.7.

The general steady-state rate law equation for the oxide

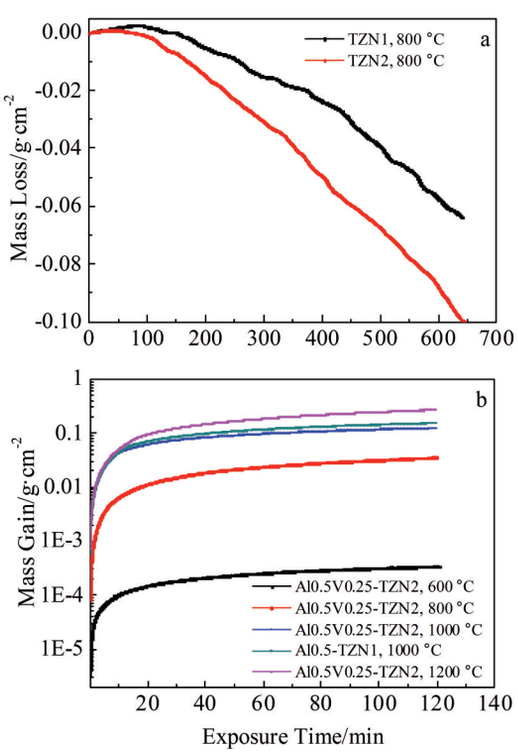


Fig.6 Corrosion behavior of different Ti-Zr-Nb alloys in high temperature steam: (a) TZN1 and TZN2 alloy; (b) Al0.5V0.25-TZN2 and Al0.5-TZN1 alloy

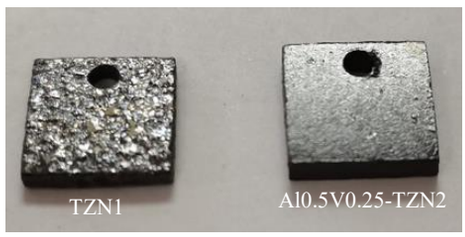


Fig.7 Surface morphologies of TZN1 alloy and Al0.5V0.25-TZN2 alloy after oxidation in steam at 800 °C

layer thickness ($x$, or an equivalent mass gain) is represented by Eq.(5)[21].

$$x^n=k_p t \quad (5)$$

The growth of the oxide layer follows a parabolic rate ($n$= 2.02±0.43 for steam) during steady-state conditions, as determined by linear regression analyses. The parabolic rate is due to the self-shielding of diffusion by the oxide scale as it thickens during growth[22]. The increase in diffusion distance during film development corresponds to a parabolic decline of the reaction rate. Therefore, using Eq. (5) and TGA measurements of mass gain, parabolic oxidation rate constants of the specimens with time ($t$) are calculated and summarized in Table 2. The reaction rate constant is a thermally dependent parameter and follows an Arrhenius relationship, as given by Eq. (6). The steady-state reaction rate constant therefore is defined by the preexponential constant ($k_0$ in $g^2 \cdot cm^{-4} \cdot s^{-1}$) and activation energy ($E_a$ in $kJ \cdot mol^{-1}$), given as follows:

$$k_p = k_0 e^{\frac{-E_a}{RT}} \quad (6)$$

where $R$ is the universal gas constant ($R$=8.314 $J \cdot K^{-1} \cdot mol^{-1}$) and $T$ is the absolute temperature.

Taking the natural logarithm for Eq. (6) and re-arranging yields:

$$\ln k_p = \frac{-E_a}{RT}\frac{1}{T} + \ln k_0 \quad (7)$$

Because the microstructure and oxidation behavior of Al0.5-TZN1 and Al0.5V0.25-TZN2 alloys are similar, regression analysis was performed using Eq. (7) by taking the reciprocal temperature as the independent variable and the natural logarithm of the parabolic oxidation rate of both alloys as the dependent variable, which have yielded activation energies of the Al0.5-TZN1 and Al0.5V0.25-TZN2 specimens of 163 $kJ \cdot mol^{-1}$ in steam environments. Fig. 8 shows a plot of the logarithm of the parabolic oxidation rate constants of Al0.5-

**Table 2 Parabolic oxidation rate constants ($k_p$) of Al0.5V0.25-TZN2 alloy and Al0.5-TZN1 alloy in steam environments**

| Alloys | $T$/K | $k_p/g^2 \cdot cm^{-4} \cdot s^{-1}$ |
|---|---|---|
| Al0.5V0.25-TZN2 | 873 | $1.63\times10^{-11}$ |
| | 1073 | $5.98\times10^{-10}$ |
| | 1273 | $5.27\times10^{-8}$ |
| | 1473 | $4.95\times10^{-8}$ |
| Al0.5-TZN1 | 1273 | $5.67\times10^{-8}$ |

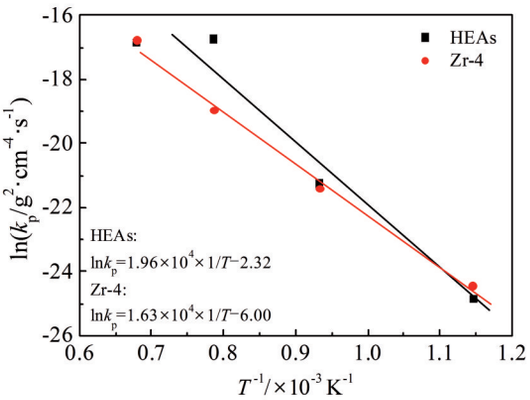


Fig.8 Parabolic oxidation rate for Al0.5-TZN1, Al0.5V0.25-TZN2 alloys and Zr-4 alloy as a function of the reciprocal temperature in steam

TZN1 and Al0.5V0.25-TZN2 alloys and Zr-4 alloy with respect to the reciprocal temperature under steam condition. Zr-4 alloy is the cladding material commonly used in reactors. The activation energy of Zr-4 is about 136 kJ·mol$^{-1}$, and the oxidation rate constants of Al0.5-TZN1 and Al0.5V0.25-TZN2 alloys and Zr-4 alloy are similar at different temperatures. Therefore, the oxidation property of Ti-Zr-Nb alloys with Al addition is comparable to that of Zr-4.

The corrosion kinetics of autoclave tested Ti-Zr-Nb samples is presented in Fig.9, with corrosion mass gain as a function of autoclave exposure time in pure water under 360 °C/18.6 MPa conditions. After exposure in autoclave for 50 d, spallation begins to arise on the surface of TZN1 and V0.25-TZN2 alloys, and as a result the rate of mass gain slows down and finally the mass begins to decrease.

For the Ti-Zr-Nb alloys with Al addition about 15at%, such as Al0.5-TZN1, Al0.5-TZN2 and Al0.5V0.25-TZN2, corrosion kinetics are almost the same before kinetic transition, which happens after 150 d. The pre-transition kinetics can be fitted to a simple power-law expression, with an exponent of 0.53 for these three kinds of alloys. For Al0.5-TZN1 and Al0.5V0.25-TZN2, corrosion rates are accelerated after transition, while for Al0.5-TZN2, after transition the oxide surface begins to spall, which decreases the mass with increasing the exposure time. Before and after kinetic transition, the oxide is black in these three kinds of samples. The difference between the post-transition corrosion behaviors of these three kinds of alloys may be because of the different microstructures of the alloys. In this study, autoclave samples are prepared from as-cast ingot, so grain size and microstructure can differ a lot in each ingot. Grain size and microstructure will affect the microstructure of the oxide layer formed during corrosion, so alloys with similar composition can behave differently during the corrosion process[23,24]. Further deformation processing such as extrusion, hot rolling or cold rolling, will make the microstructure of the alloys more homogenous.

Furthermore, the phase structures of corroded TZN1 alloy and Al0.5-TZN1 alloy were analyzed by GIXRD, as shown in Fig. 10. The oxides of TZN1 alloy and Al0.5-TZN1 alloy are determined to be (Ti, Zr)$O_2$ (Srilankite, PDF35-0584). The structure of (Ti, Zr)$O_2$ is different from that of typical $TiO_2$ (anatase, rutile and brookite) and $ZrO_2$ (baddeleyite, tetragonal and cubic). It is normally found as a product of reaction between $TiO_2$ and $ZrO_2$ during mechanical treatment such as ball milling[25,26], and is rarely observed in the oxide layer during oxidation or corrosion. This phase is found on the oxide surface of Ti-Zr-Nb HEAs, maybe because of the unique structure of HEAs.

Although XRD results show that the oxides formed on TZN1 alloy and Al0.5-TZN1 alloy are basically the same type, the mass gain and corrosion behavior of the alloys are totally different after 50 d exposure. For TZN1 alloy, the mass gain is about 50.17 mg/dm$^2$, and spallation appears on the oxide surface, while for Al0.5-TZN1 alloy, mass gain is about 28.10 mg/dm$^2$, and the oxide surface keeps integrate. These results indicate that the addition of Al can reduce the corrosion rates and promote the stability of the corrosion oxide layer. It is also reported that the addition of Al in HEAs may not affect the type of oxide, but the oxidation and

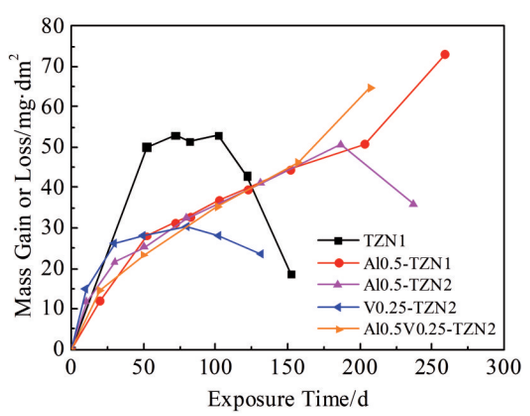


Fig.9 Corrosion behavior of different Ti-Zr-Nb alloys in water at 360 °C

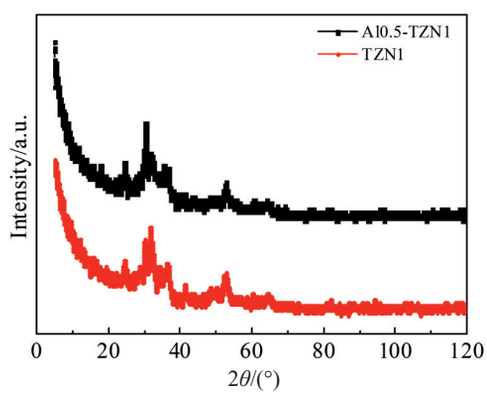


Fig.10 GIXRD patterns of Ti-Zr-Nb alloys after the autoclave testing under 360 °C/18.7 MPa for 50 d

corrosion behavior will change a lot[14]. The detailed reason for this need further research on the detail of oxide layer through TEM or X-ray photoelectron spectroscopy (XPS) analyses.

The oxide layer formed on the surface of Ti-Zr-Nb ternary alloys will spall, both during the oxidation in steam and autoclave testing process, which indicates that the oxide layers of Ti-Zr-Nb ternary alloys are unstable. The spallation of oxide layer mainly occurs on the surface of metals or alloys with high P-B ratio, which induces high stress field in the oxide layer. The oxide behavior of Ti-Zr-Nb alloys in air was investigated by different research. It is shown that the oxides formed on Ti-Zr-Nb alloys are mainly $TiNb_2O_7$, $TiO_2$, $Nb_2Zr_6O_{17}$ and $Ti_3O_5$, etc, which can hardly protect the alloys from further oxidation[27,28]. In this research, after the corrosion in 360 °C/18.6 MPa pure water, the oxide layer of Ti-Zr-Nb alloys is mainly of Srilankite type, which indicates that the corrosion medium can affect the oxidation process a lot.

In this study, it is found that addition of about 15at% Al can improve the stability of oxide layer formed in steam and 360 °C pure water, and no spallation occurs on the surface. In previous studies, $Al_2O_3$ was found in the oxide layer formed on oxidation surface, which can protect the matrix from further oxidation, and promote the oxidation resistance[28]. However, the adhesion between $Al_2O_3$ and HEAs is questionable, which may lead to the spallation of the surface layer[29]. In this study, the effect of Al on the corrosion and oxidation behavior may be caused by the formation of $Al_2O_3$. However, GIXRD results do not show the existence of $Al_2O_3$, which may be due to the low content of $Al_2O_3$ in the oxide layer. Further TEM and X-ray photoelectron spectroscopy (XPS) analysis are necessary to clarify microstructure of the oxide layer.

## 4 Conclusions

1) The crystal structure of Ti-Zr-Nb ternary alloys is basically simple bcc structure, while after addition of Al, crystal structure of Ti-Zi-Nb allays will transform to ordered B2 structure. Phase diagram shows that Al is inclined to form intermetallics with different stotchinmetries in Ti-Zr-Nb alloys, which reduces the single-phase bcc temperature region.

2) During the corrosion process in 360 °C water and high temperature (600~1200 °C) steam, the corrosion oxide layer on TiZrNb ternary alloys tends to spall during the corrosion process. An appropriate amount of Al addition (about 15at%), will increase the stability of oxide layer formed on Ti-Zr-Nb alloys in 360 °C water and high temperature steam.

3) The oxide layer growth of Ti-Zr-Nb alloys with Al addition (about 15at% ) follows a parabolic rate in high temperature steam. The activation energy of the steady-state oxidation reaction is around 163 $kJ \cdot mol^{-1}$. The activation energy and high temperature oxidation property of Ti-Zr-Nb alloys with Al addition are comparable to those of Zr-4 alloy.

4) With increasing the Al addition from 0at% to 15at%, the corrosion resistance of Ti-Zr-Nb alloys is improved for exposure in 360 °C pure water environment. With Al content about 15at% , pre-transition kinetics follows a simple parabolic law, and the corrosion transition happens after 150 d of exposure. With or without Al addition, the oxides formed on Ti-Zr-Nb alloys are mainly Srilankite type (Ti, Zr)$O_2$.

## References


1 Zinkle S J, Terrani K A, Gehin J C *et al. Journal of Nuclear Materials*[J], 2014, 448: 374

2 Yeh J W, Chen S K, Lin S J *et al. Advanced Engineering Materials*[J], 2004, 6: 299

3 Senkov O N, Senkova S V, Woodward C. *Acta Materialia*[J], 2014, 68: 214

4 Lu C Y, Niu L L, Chen N J *et al. Nature Communications*[J], 2016, 7: 13 564

5 Qiu X W, Zhang Y P, He L *et al. Journal of Alloys and Compounds*[J], 2013, 549: 195

6 Shi Y, Collins L, Feng R *et al. Corrosion Science*[J], 2018, 133: 120

7 Miracle D B, Senkov O N. *Acta Materialia*[J], 2017, 122: 448

8 Senkov O N, Miracle D B, Chaput K J *et al. Journal of Material Research*[J], 2018, 33: 3092

9 Komarov F F, Pogrebnyak A D, Konstantinov S V. *Technical Physics*[J], 2015, 60: 1519

10 Wang J, Li X, Wang J *et al. Corrosion Science*[J], 2015, 95: 125

11 Liu Y, Chen M, Li Y X *et al. Rare Metal Materials and Engineering*[J], 2009, 38(9): 1602 (in Chinese)

12 Zhou Y J, Zhang Y, Wang Y L *et al. Rare Metal Materials and Engineering*[J], 2007, 36(12): 2136

13 Kao Y F, Lee T D, Chen S K *et al. Corrosion Science*[J], 2010, 52: 1026

14 Liu Y X, Cheng C Q, Shang J L *et al. Transactions of Nonferrous Metals Society of China*[J], 2015, 25: 1341

15 Zhang W, Tang R, Yang Z B *et al. Surface and Coatings Technology*[J], 2018, 347: 13

16 Zhang Y, Zuo T T, Tang Z *et al. Progress in Materials Science* [J], 2014, 61: 1

17 Miracle D B, Miller J D, Senkov O N *et al. Entropy*[J], 2014, 16: 494

18 Takeuchi A, Inoue A. *Materials Transactions*[J], 2005, 46(12): 2817

19 Li W D, Xie D, Li D Y *et al. Progress in Materials Science*[J], 2021, 118: 100 777

20 Ding Q Q, Zhang Y, Chen X *et al. Nature*[J], 2019, 574: 223

21 Pieraggi B. *Oxidation of Metals*[J], 1987, 27(3-4): 177

22 Atkinson A. *Materials Science and Technology*[J], 1988, 4(12): 1046

23 Zhang X Y, Shi M H, Li C *et al. Materials Science and Engineering A*[J], 2007, 448: 259

24 Ralston K D, Birbilis N. *Corrosion*[J], 2010, 66: 75 005

25 Kraleva E, Spojakina A, Saladino M L *et al. Journal of Nanoscience and Nanotechnology*[J], 2010, 10: 8417

26 Kong L B, Ma J, Zhu W *et al. Journal of Alloys and Compounds*

[J], 2002, 335: 290
27 Butler T M, Chaput K J, Dietrich J R *et al. Journal of Alloys and Compounds*[J], 2017, 729: 1004
28 Cao Y K, Liu Y, Liu B *et al. Transactions of Nonferrous Metals Society of China*[J], 2019, 29: 1476
29 Chen J, Zhou X Y, Wang W L *et al. Journal of Alloys and Compounds*[J], 2018, 760: 15

# Al对低中子吸收截面Ti-Zr-Nb高熵合金的微观结构和腐蚀行为的影响

贾玉振[1]，侯雅青[2]，王朋飞[1]，张　伟[1]，戴　训[1]
(1. 中国核动力研究设计院 反应堆燃料及材料重点实验室，四川 成都 610213)
(2. 中国钢研科技集团有限公司 数字化研发中心，北京 100081)

**摘　要：**针对Al对低中子吸收截面Ti-Zr-Nb系高熵合金的微观结构和腐蚀行为进行了研究。比较了不含Al和含15at%Al的Ti-Zr-Nb合金的相图、微观结构、氧化行为和腐蚀行为。相图计算结果表明，在熔点下Ti-Zr-Nb三元合金为bcc相，添加的Al会倾向于在合金中形成不同的金属间化合物，而缩小相图中bcc单相区的温度区。XRD和TEM结果表明，熔炼获得的Ti-Zr-Nb三元合金为简单的bcc结构，而Al会导致晶体结构转变为有序的B2结构。通过热重分析和高压釜试验对Ti-Zr-Nb系高熵合金的腐蚀行为进行了研究。结果表明，在腐蚀过程中，Ti-Zr-Nb三元合金的氧化膜容易发生剥落，而添加Al会提高氧化层的稳定性，但不会改变腐蚀氧化层的主要氧化物种类。通过计算反应速率常数和激活能对氧化动力学进行了研究，发现添加Al的Ti-Zr-Nb系合金的高温氧化性能与Zr合金接近。

**关键词：**Ti-Zr-Nb合金；Al；高熵合金；腐蚀；氧化

---

作者简介：贾玉振，男，1988年生，博士，副研究员，中国核动力研究设计院反应堆燃料及材料重点实验室，四川 成都 610213，电话：028-85903839，E-mail：jaja880816@aliyun.com